LA-UR-17-24219 (Accepted Manuscript)

Interface structures and twinning mechanisms of twins in hexagonal metals

Gong, Mingyu
Hirth, John
Liu, Yue
Shen, Yao
Wang, Jian

To be published in: Materials Research Letters

DOI to publisher's version: 10.1080/21663831.2017.1336496

Permalink to record: http://permalink.lanl.gov/object/view?what=info:lanl-repo/lareport/LA-UR-17-24219

Materials Research Letters

ISSN: (Print) 2166-3831 (Online) Journal homepage: http://www.tandfonline.com/loi/tmrl20

Interface structures and twinning mechanisms of twins in hexagonal metals

Mingyu Gong, John P. Hirth, Yue Liu, Yao Shen & Jian Wang

To cite this article: Mingyu Gong, John P. Hirth, Yue Liu, Yao Shen & Jian Wang (2017): Interface structures and twinning mechanisms of twins in hexagonal metals, Materials Research Letters, DOI: 10.1080/21663831.2017.1336496

To link to this article: http://dx.doi.org/10.1080/21663831.2017.1336496

Published online: 07 Jun 2017.

MATER. RES. LETT., 2017
https://doi.org/10.1080/21663831.2017.1336496

MATERIALS RESEARCH LETTERS
Taylor & Francis
Taylor & Francis Group

ORIGINAL REPORT

Interface structures and twinning mechanisms of $\{\bar{1}012\}$ twins in hexagonal metals

Mingyu Gong[a], John P. Hirth[b], Yue Liu[b,c], Yao Shen[c] and Jian Wang [a,d]

[a]Department of Mechanical and Materials Engineering, University of Nebraska-Lincoln, Lincoln, NE, USA; [b]Materials Science and Technology Division, Los Alamos National Laboratory, Los Alamos, NM, USA; [c]State Key Lab of Metal Matrix Composites, School of Materials Science and Engineering, Shanghai Jiao Tong University, Shanghai, People's Republic of China; [d]Nebraska Center for Materials and Nanoscience, University of Nebraska-Lincoln, Lincoln, NE, USA

ABSTRACT

A controversy concerning the description of $\{\bar{1}012\}\langle 10\bar{1}1\rangle$ twinning, whether it is shear-shuffle or pure glide-shuffle or pure shuffle, has developed. There is disagreement about the interpretation of transmission electron microscopic observations, atomistic simulations and theories for twin growth. In this article, we highlight the atomic-level, characteristic, equilibrium and non-equilibrium boundaries and corresponding boundary defects associated with the three-dimensional 'normal', 'forward' and 'lateral' propagation of $\{\bar{1}012\}$ growth/annealing and deformation twins. Although deformation twin boundaries (TBs) after recovery exhibit some similarity to growth/annealing TBs because of the plastic accommodation of stress fields, there are important distinctions among them. These distinctions distinguish among the mechanisms of twin growth and resolve the controversy. In addition, a new type of disconnection, a glide disclination, is described for twinning. Synchroshear, seldom considered, is shown to be a likely mechanism for $\{\bar{1}012\}$ twinning.

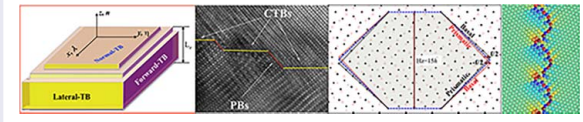

IMPACT STATEMENT

A controversy concerning $\{\bar{1}012\}\langle 10\bar{1}1\rangle$ twinning in hcp metals has developed. We present comprehensive understanding of interface structures and twinning mechanisms of $\{\bar{1}012\}$ growth/annealing and deformation twins at the atomic level.

ARTICLE HISTORY
Received 4 March 2017

KEYWORDS
Twin; boundary; disclination; synchroshear; hexagonal materials

1. Introduction

Crystal twins form by three modes. Growth twins form by the nucleation of faulted layers in growth by solidification or during vapor deposition [1–5]. Annealing twins form similarly during recrystallization and grain growth [6,7]. Both processes occur at relatively low driving forces and hence low growth rates, $\dot{G}$ and the faulting probability is related to relative nucleation rates, $\dot{N}$: hence $\dot{N}/\dot{G}$ is large [8]. They also typically occur where the thermally controlled relaxation of the interface structure, say by dislocation emission, is relatively easy and where final interfaces tend to be in near-equilibrium configurations [7–10]. The third mode is deformation twinning. This typically occurs at low temperatures, and under large driving forces but where nucleation is athermal, and hence where $\dot{N}/\dot{G}$ is small [8,11]. For example, in the pole mechanism [12–16], once a twin nucleus forms it propagates rapidly. The thermally controlled relaxation of the interface is difficult so that final interfaces tend to be far-from-equilibrium.

The consequences are that the growth or annealing twins contain more than one type of defect [8]: several types of twinning disconnections (TDs, also called twinning dislocations) [17,18] or disclinations [19] or a

CONTACT Jian Wang jianwang@unl.edu Department of Mechanical and Materials Engineering, University of, Nebraska-Lincoln, Lincoln, NE 68588, USA, Nebraska Center for Materials and Nanoscience, University of Nebraska-Lincoln, Lincoln, NE 68588, USA; Yao Shen yaoshen@sjtu.edu.cn State Key Lab of Metal Matrix Composites, School of Materials Science and Engineering, Shanghai Jiao Tong University, Shanghai 200240, People's Republic of China

mixture of TDs and interface dislocations [20–24]. The TDs are characterized by a Burgers vector $\boldsymbol{b}$ and a step height h [17,25–27]. They also have a blocky, nominally equiaxed shape [6,7,28]. In contrast, deformation twins often contain only one type of TD and have associated elastic strain fields. They also tend to have highly asymmetric lenticular shapes [29]. Hence, observable boundaries always have some defects present aside from the perfect terrace planes. A special category is a nucleus, which is completely bounded by coherent terraces as in the usual nucleation models [30–32].

Thus, there are several types of twin boundaries (TBs) associated with these twins. We focus on twins formed by TD glide, where the perfect twin plane or terrace is parallel to K_1 and the shear direction is $\boldsymbol{\eta}||\boldsymbol{\eta}_1$. Also, the normal to K_1 is $\boldsymbol{n}$ and the lateral direction is parallel to $\boldsymbol{\lambda} = \boldsymbol{\eta} \times \boldsymbol{n}$. Corresponding to the three-dimensional growth of a blocky twin, three types of TBs form for the 'normal' (parallel to $\boldsymbol{n}$), 'forward' (parallel to $\boldsymbol{\eta}$) and 'lateral' (parallel to $\boldsymbol{\lambda}$) propagation directions, the three boundaries are referred to as normal-TB, forward-TB and lateral-TB, shown in Figure 1(a). TBs associated with $\{\bar{1}012\}$ twins can be observed at the atomic level, using high-resolution transmission electron microscope (HRTEM), when the beam direction is parallel to the vector $\boldsymbol{\lambda}$. Thus, we refer to the view of the twin domain along the vector of $\boldsymbol{\lambda}$ as the 'bright side (BS)' of the twin (Figure 1(b)) [33]. The normal-TB and the forward-TB can be identified in the BS view of a twin at the atomic level. When the twin domain is observed along the twinning direction $\boldsymbol{\eta}$, the twin domain is crystallographically indistinguishable from the matrix in HRTEM because of the identical projection of both twin and matrix crystals (Figure 1(c)), though it can be observed using low-resolution transmission electron microscope (TEM) because of the strain contrast around TBs. We thus refer to the view of the twin domain along the twinning shear direction as the dark side view (DS) of the twin [33]. The lateral-TB and normal-TB can be characterized in the DS view of a twin. The top view of a twin along the normal $\boldsymbol{n}$ to K_1 (Figure 1(d,e)) shows the twin shape and characters of TDs, edge in the forward-TB and screw or mixed in the lateral-TB.

Initial crystallographic theory [16] focused on deformation twins and defined possible TDs for a given twin system. Bilby and Crocker [34] later defined the shuffles necessary to complete a twinning transformation via TDs. See also the reviews in [35,36]: we refer to the models in [6,11,35,36] as the classical model. These are incorporated in the topological model (TM) as recently reviewed [8,17,27,37]. There are many observations of twinning that are consistent with this TD-shear-shuffle model [24,38–43]. A controversy, whether twinning is shear-shuffle or pure glide-shuffle or pure shuffle, has developed concerning the description of $\{\bar{1}012\}\langle 10\bar{1}1\rangle$ twinning in hexagonal close packed (hcp) metals, the most commonly activated system under tension along the c-axis in Mg, Ti, Zn, Zr and Co [22,42–46]. This system is interesting in that the shuffle vectors $\boldsymbol{s}$ are much larger than the Burgers vectors $\boldsymbol{b}_t$. Yet, there is much evidence [24,40,43,47,48,50] that the conventional TD-shear-shuffle mechanism still applies, dating back to the analysis of Thompson and Millard [16]. However, an alternative general (pure) shuffle mechanism has been proposed [49], based on HRTEM observations of prism/basal (P/B) facets at TBs. This mechanism is questionable since, as discussed in the following, the P/B facets usually produce coherency stresses and do not

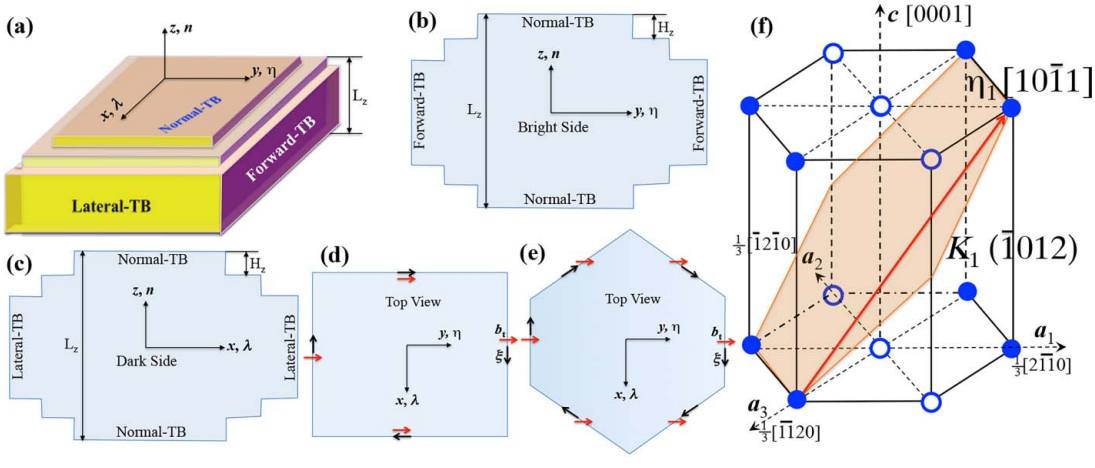

Figure 1. (a) A 3-D 'cube' view of a twin domain with $x||\boldsymbol{\lambda}$, $y||\boldsymbol{\eta}$, and $z||\boldsymbol{n}$; and the thickness L_z. (b) A BS view of the twin with steps that are normal to $\boldsymbol{\eta}$ and have step height H_z. (c) A DS view of the twin with steps that are normal to $\boldsymbol{\lambda}$ and have step height H_z. (d) and (e) A top view of the twin showing a rectangular shape (d) or a hexagonal shape (e). The red arrows indicate the Burgers vector of twinning dislocations, and the black arrows indicate the line sense of twinning dislocations. (f) Coordinates for hcp structure.

retain crystallographic mirror symmetry [41,50]. Here we show that a pure glide-shuffle mechanism, associated with pure steps and differing from a pure shuffle mechanism [14], is possible and is consistent with the TM. Usually, these steps are paired with TDs with both step and dislocation character, producing a shear-shuffle mechanism. Recovery mechanisms also can have a role in forming pure steps.

The earliest geometrical model of the $\{\bar{1}012\}$ twin was derived by Thompson and Millard [16] and predicted the shear caused by the twin. Many studies of such twinning entail viewing a limited number of one type of TB. Yet as noted above, there are many possible boundaries. Hence we present here a systematic set of observations of the different types of TBs, including near-equilibrium and far-from-equilibrium examples. We select the $\{\bar{1}012\}\langle 10\bar{1}1\rangle$ system because of the importance of shuffles and because of the large amount of work on this system.

2. Types of interface defects

2.1. Equilibrium defects

A planar terrace or coherent twin boundary (CTB) is at equilibrium except at very high temperatures where entropic roughening is possible. A TB with a regular array of TDs together with interface dislocations can be at elastic equilibrium [14]. The net in-plane Burgers vector content **B** must be zero. The net $\mathbf{B}_y$, i.e. the total Burgers vector content normal to the interface, produces tilt but no long-range strain in a bi-crystal. However, for a twin domain embedded in the matrix, this cannot be accomplished by a single type of defect, but can be produced by TDs with several Burgers vectors [8], by a set of interface dislocations with different Burgers vectors [50,51], or by a combination of interface dislocations and TDs [33]. Finally, pure steps have no long-range strain field [18].

2.2. Non-equilibrium defects

We classify types of defects associated with twins and then give specific examples in the sections to follow. First, unit TDs, those of minimum step height, unless part of a uniform array on terrace or planar facets, have elastic strain fields and are non-equilibrium defects by definition. The same is true for interface dislocations. PB or BP facets that bond basal and prismatic planes (the first character, B or P, represents the twin plane and the second character represents the matrix plane) on a TB represent a pair of disclination dipoles with associated strain fields that can be large [8,19]. More subtly, domain defects at corners of boundaries often have some dislocation character and associated strains [8,52–54]. In particular, this is true for coherent twins at or near the critical size for twin nucleation [32]. For a twin domain embedded in a matrix, a TB with a regular array of TDs is at non-equilibrium. If the twin terminates without accommodation, the net $\mathbf{B}_y$, Burgers vector content normal to the interface, produces long-range strain.

2.3. Twinning disconnections

The TD associated with $K_1 = \{\bar{1}012\}$ twins has step $H = 2h$, i.e. two planes, as shown in the coherent dichromatic pattern (CDP) in Figure 2(a). A matrix unit cell (right) and a twin unit cell (left) are also depicted. The shortest lattice vector $[\bar{1}011] = [10\bar{1}1]_T$ is equal to a perfect dislocation Burgers vector $\boldsymbol{b}_0$ in either lattice. The coherent dichromatic complex (CDC) in Figure 2(b) shows the shuffles that complete the transformation. The repeatable e-cell, also shown, contains all necessary information [8,41]. Of importance for later detailed analysis,

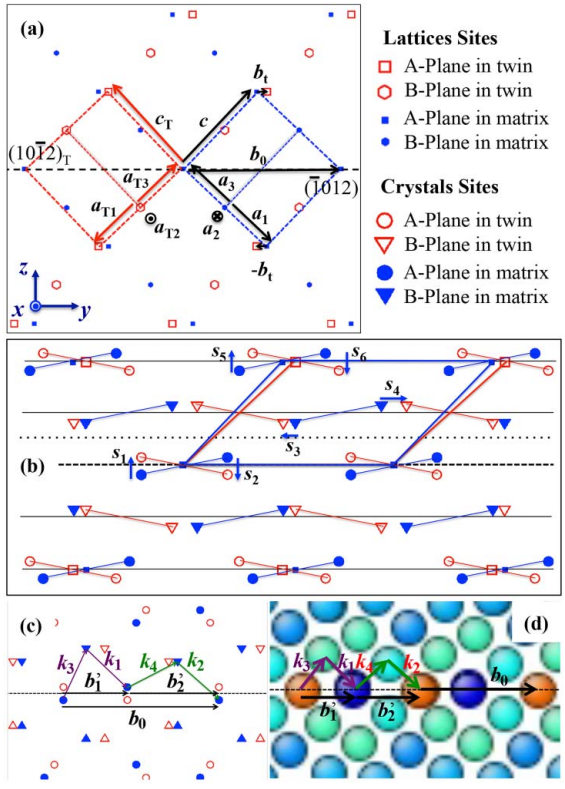

Figure 2. Dichromatic constructions for $(\bar{1}012)[10\bar{1}1]$ twin in Mg. (a) CDP. Solid symbols are lattice sites in matrix, open ones in twin. Large symbols in one plane, small ones in adjacent plane. (b) CDC. Basis pairs connected by thin dashed lines, dividing surface indicated by heavy dashed line, commensurate plane by dotted line. The arrows indicate shuffle displacement. An e-cell is denoted by solid lines. (c) Vectors related to synchroshear shown in CDC. (d) The actual relaxed interface of $(\bar{1}012)$ TB in Mg. $\boldsymbol{\xi}$ points toward the reader.

the vector is the sum of four a-type vectors, two in the matrix and two in the twin (Figure 2(a)). In the matrix, the a_T vectors become imperfect vectors of the type $1/6[4\bar{2}\bar{2}3]$ and differ in length. For later reference, the Burgers vectors $\boldsymbol{b}_1' = 1/2[10\bar{1}1]$ and $\boldsymbol{b}_1' = 1/2[\bar{1}011]_T$ and second pair should be $\boldsymbol{b}_2'$ (equal to $\boldsymbol{b}_1'$). Kronberg vectors $\boldsymbol{k}_1$, $\boldsymbol{k}_2$, $\boldsymbol{k}_3$, $\boldsymbol{k}_4$ of the a and a_T type are shown in a reference dichromatic complex (Figure 2(c)) and the actual relaxed interface (Figure 2(d)). As seen there, the actual interface $\boldsymbol{k_i}$ vectors are more regularly and more symmetrically arranged, and shuffles near the interface tend to be suppressed. Moreover, in the actual interface the spacings relax so that both Burgers vectors become the average length $\boldsymbol{b}_1 = 1/2[10\bar{1}1]$.

The Burgers vector of the twinning dislocation is about $1/15[10\bar{1}1]$ for Mg [51]. In atomistic simulations, a deformation twin can be created in a single crystal through the gliding and shuffling associated with TD motion: (i) TDs glide on every two atomic planes, and all atoms in the model are first displaced according to the dislocation displacement field of a TD; and (ii) atoms in the twin domain are then displaced according to the shuffle displacement field. This is equivalent to separately considering the displacements of the pure step component and those of the dislocation and then adding them. This method has been programmed for simulations of dislocations and twins in face-centered cubic (fcc) and body-centered cubic structures [55,56], and extended for dislocations and twins in hcp structure [57]. After a TD glides, remote atoms above and below the shear plane experience a relative displacement of $\boldsymbol{b}_t$. (All displacements can be represented in the e-cell, which are also shown in Figure 2(b)). The displacements in the e-cell or the relative displacements in the entire system are unique [8,41]. However, the position of the interface, and how the displacements are divided into shears and shuffles can be represented in different ways [41]. The method selected here is the same as [8]. The magnitude of the Burgers vector of the TD is 0.0488 nm for Mg. There are three atomic layers and four atoms in the e-cell (Figure 2(b)). The different shuffle vectors/displacements are $\boldsymbol{s}_1 = [0\ 0\ 0.03154]$, $\boldsymbol{s}_2 = [0\ 0\ -0.03154]$, $\boldsymbol{s}_3 = [0\ -0.04268\ 0]$, $\boldsymbol{s}_4 = [0\ 0.09197\ 0]$, $\boldsymbol{s}_5 = [0\ 0\ 0.03154]$, $\boldsymbol{s}_6 = [0\ 0\ -0.03154]$ for Mg.

2.4. Disclinations

In the hcp system, arrays of TDs often relax into a PB or BP facet, as demonstrated in numerous experimental observation and MD simulations [21,22,30,31,58–67]. These facets correspond to disclination dipoles [26,30,59]. The disclination characteristics have been analyzed in a version of the TM [19,39]. This disclination description is augmented in [8] to include discussion of various disclination multipoles. The latter analysis also adheres to the dichromatic approach [26] rather than to the trichromatic version in [39], although the results are the same. Examples of several types of disclinations are treated below. Pairs of non-collinear disclinations are also observed to meet at corners, forming a domain disclination [26].

3. Growth and annealing twins

3.1. Normal TBs

The growth and annealing twins tend to be bounded by equilibrium TBs and are similar; so we discuss them together briefly as growth twins. The normal TBs usually have perfect twin planes or large perfect terraces, as observed in nanotwinned Cu foils in Figure 3(b) and in hcp Co in Figure 3(d). The blocky equilibrium twins tend to be nominally equiaxed as in Figure 3(a,c) and illustrated in Figure 1(e).

3.2. Forward TBs

3.2.1. Stressed forward TBs and steps

The forward-TB must have a fixed minimum length if it is to be stress free. In fcc, this is easily accomplished by alternating TDs with three different Shockley partial dislocations that sum to zero (Figure 4(a,b)) [2,70]. Such 3-layer twins have been observed in HRTEM [2,68,71] and large twins with equilibrium structures formed by such TD motion have been observed [72]. Thus, for fcc,

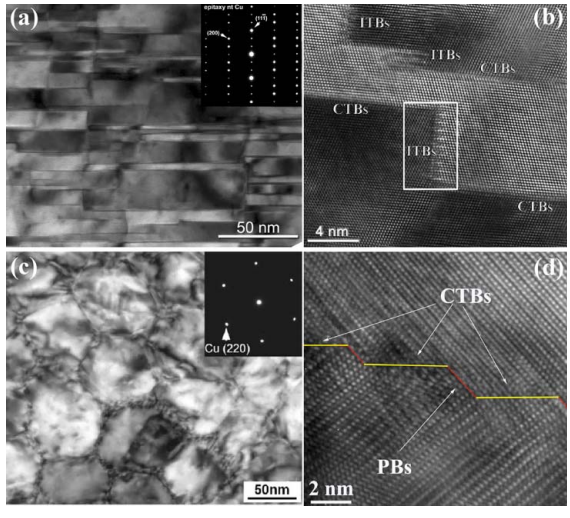

Figure 3. Nanotwinned Cu films fabricated by physical vapor deposition, showing (a) BS view of twins, (b) atomic structures of the (111) CTB and {112} steps (incoherent TB) [2,68], and (c) top view of hexagonal twins [69]. (d) HRTEM image of $(10\bar{1}2)$ serrated CTB plus PB steps in Co [22].

the length L_z for Figure 1 must have a step height $3jh$, where h is the unit step height equal to the interplanar spacing of {111} planes and j is an integer. Thus, the minimum value of H_z for a stress-free structure is $3h$. Similarly, for a stress-free step, the step height in Figure 1 must be $H_z = 3jh$. There can be more than one type of interface structure produced by glide-shuffle. For example, a $3h$ step normal to a (111) plane could have successive partials Aδ, Bδ and Cδ, or, alternatively, Aδ, Aδ, $-$2Aδ. The former is stable, and the latter is metastable [2]. In annealing twins, equilibrium steps can be quite large, up to several micrometers [6,7,28]. The relaxed step or twin end can be envisioned to have been a stressed array that relaxes by the addition of misfit partials with other Burgers vectors that cancel the stress fields. This approach is useful for hcp, where we first consider stressed arrays and then how they relax.

The situation is more complicated for hcp. The dichromatic patterns for a $(\bar{1}012)$ twin viewed in the $-\boldsymbol{\lambda} = [\bar{1}2\bar{1}0]$ direction are depicted in Figure 4(c). The minimum step height, i.e. the minimum height twin or step that can relax to become stress free, varies with c/a ratio. With Mg as an example the minimum value of H_z or L_z is $15jh$, where j is an integer and $h = d_{(10\bar{1}2)}$. When such a twin contains $(15j + m)$ planes, it will be subjected to the engineering elastic shear strain, $\gamma_{yz} = \boldsymbol{f}_m/(15j + m)h_{(10\bar{1}2)}$, where $\boldsymbol{f}_m$ is a shift vector, shown below to be

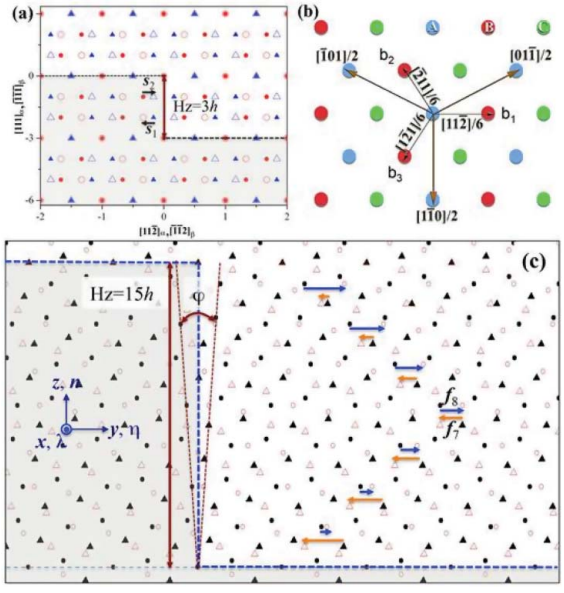

Figure 4. (a) CDP for Σ3(111) twin showing a 3-layer step and the shuffle vectors $\boldsymbol{s}_1$ and $\boldsymbol{s}_2$. (b) Plan view of (111) plane stacking and three partials $\boldsymbol{b}_1$, $\boldsymbol{b}_2$, $\boldsymbol{b}_3$. (c) CDC for a $(10\bar{1}2)$ twin viewed in the $-\boldsymbol{\lambda} = [\bar{1}2\bar{1}0]$ direction. Unlike (a), the unit cells of the matrix and twin are relatively rotated by the angle 93.71 degrees about $\boldsymbol{\lambda}$, creating a disclination (misorientation) angle φ of 3.71 degrees. $\boldsymbol{\xi}$ points toward the reader.

Table 1. The minimum step height integer j, disclination angle φ, and misfit dislocation spacings d for all hcp metals.

Metal	a	c	$2h$	j	φ	d_0	d_{45}
Cd	2.972	5.605	3.791	11	4.87	44.5	30.21
Zn	2.659	4.936	3.367	13	3.97	48.5	33.18
Co	2.502	4.061	2.963	15	3.72	45.6	33.33
Mg	3.203	5.200	3.794	15	3.71	58.6	42.78
Re	2.76	4.458	3.260	13	4.00	46.6	34.18
Zr	3.231	5.147	3.788	11	4.79	45.2	33.39
Ti	2.95	4.683	3.452	11	4.99	39.6	29.26
Hf	3.194	5.051	3.730	9	5.21	40.9	30.34
Be	2.281	3.576	2.651	9	5.7	26.6	19.79

the Frank vector, and varies with the integer m. Here, $\boldsymbol{f}_m = 0$ when $m = 0$ or 15, $\boldsymbol{f}_m = m\boldsymbol{b}_t/2$ when m is even number (2, 4, ... 14), and $\boldsymbol{f}_m = -(15\text{-}m)\boldsymbol{b}_t/2$ when m is odd (1, 3, ... 13). $\boldsymbol{b}_t$ is the Burgers vector of the twinning dislocation. The step structure in Figure 4(c) is more complicated in terms of defect character because of the relative rotation at the step, and is discussed later. Table 1 summarizes the minimum step height for all hcp metals.

An example of this kind is discussed for a nucleus for a $(\bar{1}012)$ twin in [50]. According to crystallographic analysis, there are three typical interfaces: CTBs, coherent PB boundaries (CPBs) and coherent BP boundaries (CBPs). Figure 5(a) shows an inclined interface that bonds basal and prismatic planes, referred to as BP or PB facets (they are the same in terms of the crystallography). The order has the meaning that the first character, B or P, represents the twin plane and the second character represents the matrix plane. The crystallographic mismatch is described as a Frank vector, associated with the BP or PB step, which has disclination dipole character with an associated rotation angle of $\varphi = 3.71°$ for Mg [8,19]. The disclination is characterized by either (or both) the Frank vector $\mathbf{f}$ or the angle φ. The dipole consists of the disclination at one end and an opposite sign disclination at the other with Frank vectors $\mathbf{f}$ and $-\mathbf{f}$ separated by the length L of the dipole. Represented as a dislocation array, The Frank vector $\mathbf{f}$ is bL/D, with D the dislocation spacing: i.e. $\mathbf{f}$ is the total dislocation content in the length L. For unit disconnections, or at distances large compared to L, the disclination can be represented by a single dislocation with Burgers vector $\mathbf{f}$ acting at L/2. For most cases, the content can be envisioned [8] as a partitioned pair of vectors $+/-$ $\mathbf{f}/2$ acting at L/4 and 3L/4. For the disclination dipole in Figure 5(a), each component $\mathbf{f}$ can be decomposed into a wedge component $\mathbf{f}_w$ ($=\mathbf{f}\cos\theta$) and a glide component $\mathbf{f}_g$ ($=\mathbf{f}\sin\theta$). Here, the angle θ is equal to 45°. (*Traditionally disclinations are considered to have two types* [73,74] *called wedge* [75] *and twist* [76], *see also* [77] *for other nomenclature. These correspond to a uniform tilt, edge dislocation array and a uniform screw*

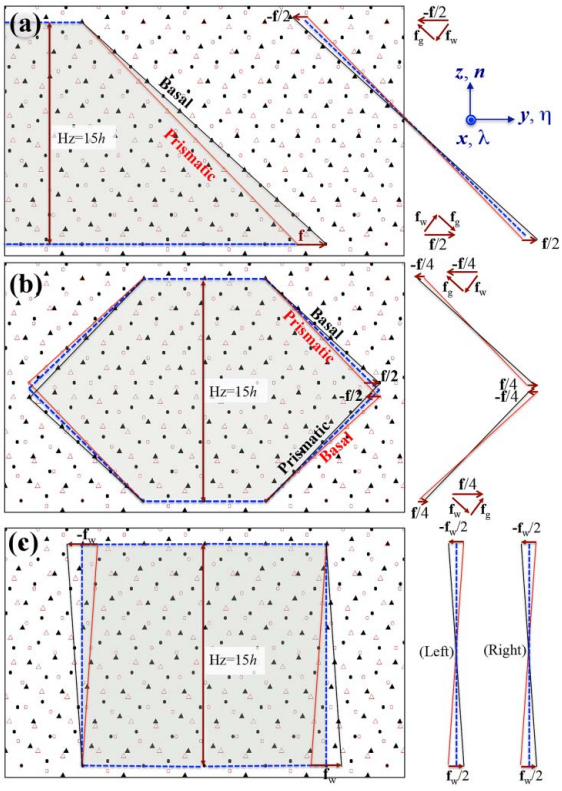

Figure 5. CDCs for a $(\bar{1}012)$ twin viewed in the $-\boldsymbol{\lambda} = [\bar{1}2\bar{1}0]$ direction, showing three type of forward boundaries: (a) an inclined boundary bonding the prismatic and basal planes that have a disclination angle of $\varphi = 3.71$ degrees, (b) two inclined boundaries with characteristic angles of $\varphi = 3.71$ and -3.71 degrees meeting at a domain disclination. (c) A vertical boundary bonding two inclined $\{\bar{1}012\}$ twin planes that subtend an angle of $\varphi = 7.42$ degrees. The blue dashed lines indicate the boundary. The thin black and red lines indicate basal and prismatic planes in (a) and (b), and represent $\{\bar{1}012\}$ planes in (c). The arrows marked by **f** are Frank vectors; the arrows marked by $\mathbf{f}_w$ and $\mathbf{f}_g$ are the wedge and glide components of the Frank vector. $\boldsymbol{\xi}$ points toward the reader.

dislocation array, respectively. However, when a facet or terrace has in-plane misfit, the field is equivalent to a disclination with a glide edge dislocation array. We define this as a ***glide disclination****.*) Hence, the glide component is smeared on the coherent BP or PB interface, with the stress source at the ends (corners) and coherency stress along the BP or PB interface. The details are shown later in Figure 6. Figure 5(b) shows a stepped interface that bonds two pairs of basal and prismatic planes, referred to as PB/BP serrated interface. The two segments of the interface have disclination dipole character with an associated rotation angle of $\varphi = 3.71°$ for Mg. Partitioning into two mixed disclinations, with both wedge and glide character, reduces the local stress fields that would be associated with one Frank vector **f** in Figure 5(b). There is a vertical boundary (Figure 5(c)) that bonds two $\{10\bar{1}2\}$ planes, referred to as a 90° tilt boundary, that also has disclination dipole character (pure wedge disclinations) with an associated rotation angle of $\varphi = 7.42$. Molecular static calculations with an empirical interatomic potential further reveal that the coherent BP/PB has a lower formation energy (111 mJ/m^2) than the CTB (122 mJ/m^2) [32]. Thus, the PB/BP serrated interface would be energetically favored because of the low interface energy and the redistribution of the Frank vector into components.

3.2.2. Relaxed forward TBs, steps

Figure 6(a) shows a twin nucleus with the minimum thickness for Mg. Initially, a 15-atomic planes thick, stressed twin ($j = 1$) is surrounded by two CTBs, two CPBs and two CBPs. With minimum twin height, the stresses can be relaxed by the addition of an imperfect dislocation. Such a twin or step moves by the collective glide of TD arrays and the imperfect dislocation analogous to the mechanism described previously for an fcc twin with height $3jh$, i.e. a glide-shuffle mechanism. The

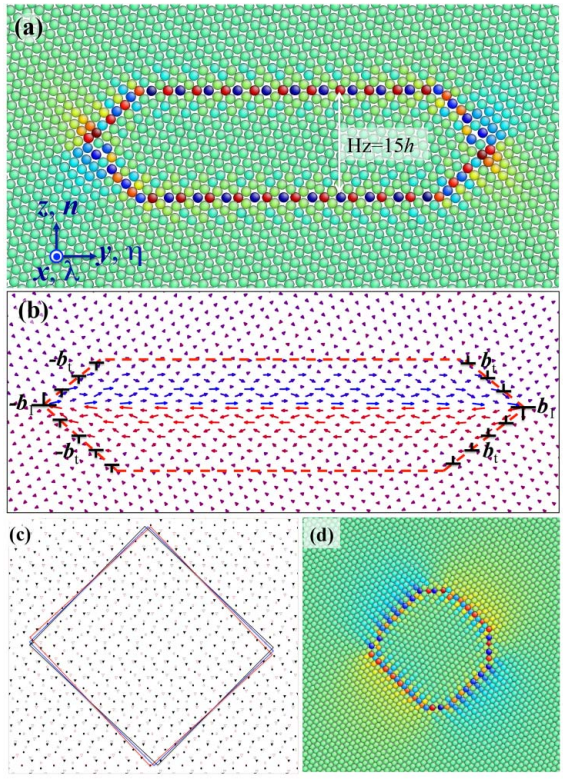

Figure 6. (a) Atomic structure of a 15-layer thick twin. Atoms are colored according to their hydrostatic pressure. Stress concentrations are clear in the corners. (b) Displacements plot of atoms in association with the formation of the zero shear strain twin. This is can be described by seven twinning dislocations and one partial dislocation. The relative shear in the matrix across the twin is equal to zero. (c) A twin nucleus outlined by PB and BP boundaries, and (d) the corresponding atomic structure. Coherency stresses are observed along PB and BP boundaries. $\boldsymbol{\xi}$ points toward the reader.

corner at the intersection of two PB and BP facets, which has higher energy than other regions, is a domain disclination that is the superposition of the two corresponding disclination dipoles. Figure 6(b) shows the atomic displacements associated with the formation of the twin. The net shear displacement in the matrix across the twin domain is very close to zero. The gliding array consists of seven TD vectors ($\boldsymbol{b}_t$) and one imperfect misfit dislocation $\boldsymbol{b}_1'$. The Burgers vector $\boldsymbol{b}_t$ has the magnitude of $a(3-\kappa^2)/\sqrt{3+\kappa^2} = 0.049$nm for Mg, along the twinning direction. Here $\kappa = c/a$. The Burgers vector $\boldsymbol{b}_1'$ has the magnitude of $a\kappa^2/\sqrt{3+\kappa^2}$ along the opposite twinning direction, 0.355 nm for Mg [50]. The net Burgers vector of the eight dislocations is essentially equal to zero. For a 30 plane thick twin, there would be 15 TDs and a perfect dislocation $\boldsymbol{b}_0$. The Burgers vector $\boldsymbol{b}_0$ has the magnitude $a\sqrt{3+\kappa^2}$, 0.759 nm for Mg. This can be rationalized as follows: after 7 TDs glide, a 14-layer twin forms; a partial $\boldsymbol{b}_1'$ glides above the TB toward the opposite twinning direction, resulting in the migration of the TB upwards one atomic layer. So, a 15-layer twin forms and the net shear is equal to zero. Then, 8 TDs glide to thicken the twin to 31 atomic planes. A partial dislocation $\boldsymbol{b}_2'$ glides below the TB to migrate the TB downwards one atomic plane. A 30-layer twin then forms and the net shear is equal to zero. The Burgers vector $\boldsymbol{b}_2'$ has the magnitude of $3a/\sqrt{3+\kappa^2}$ along the opposite twinning direction, 0.404 nm for Mg [50]. $\boldsymbol{b}_1'$ and $\boldsymbol{b}_2'$ are defined in the CDC, Figure 2(c), and have been discussed in [50]. Once in the boundary, the defects partition [78] so that they have the same Burgers vector $\boldsymbol{b}_1 = \boldsymbol{b}_1' + 1/2\boldsymbol{b}_t = \boldsymbol{b}_2' - 1/2\boldsymbol{b}_t$. Thus, subsequently, we only refer to $\boldsymbol{b}_1$. Between A and B layers, where A and B are the subsets in the basis pair, in an upward sense, the misfit dislocation glides between B and A. This is the reason that $\boldsymbol{b}_1'$ and $\boldsymbol{b}_2'$ are asymmetric relative to the TD array. As a consequence, $\boldsymbol{b}_1$ separates PB terraces that differ from one another but which are energetically degenerate.

Evidently, pure steps relax by the same mechanism. Motion of the pure steps is by shuffle: the array produces no net shear displacement. Since $\mathbf{B} = \mathbf{0}$, there is no Peach–Koehler force for the motion of pure steps. However, there is a thermodynamic driving force associated with a change in strain energy accompanying step motion [8,79]. The presence of glide-shuffle as the shuffle mechanism, see Figure 23-5c in [14], is important. It ensures that the activation energy for a single atom shuffle is small (large atom separation at a bond across the twin plane) and it results in maintaining a low index-low energy terrace plane if the step moves. In other words, it is consistent with the TM [37] and/or the crystallographic models [34] for TDs. A large vertical step with the fully relaxed structure is shown in Figure 7(a,b), where

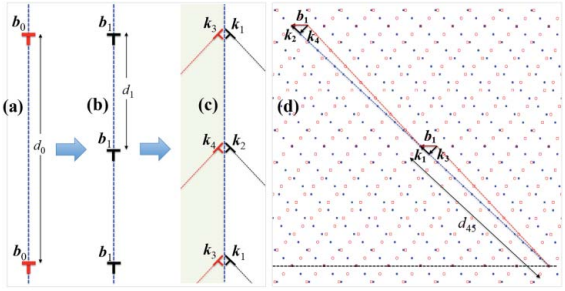

Figure 7. Stress-free interfaces, (a–c) defects in 90° tilt boundary and (d) defects in 45° PB boundary. $\boldsymbol{\xi}$ points toward the reader.

imperfect $\boldsymbol{b}_1$ dislocations relax misfit. The $\boldsymbol{b}_t$ dislocations are subsumed as the coherent Bilby terrace structure. The array of $\boldsymbol{b}_1$ dislocations can be regarded as a tilt array of grain-boundary dislocations (Figure 7(b)), or be considered to form by the superposition of two a-type dislocations $\boldsymbol{a}$ and $\boldsymbol{a}_T$ (or the combination of $\boldsymbol{k_i}$ vectors, Figure 7(c)) from the twin and matrix domains. As implied in Figure 5, a large PB facet can similarly be relaxed by an array of mixed $\boldsymbol{b}_1$ dislocations.

In principle, the step motion could occur by pure shuffle, Figure 23-5d in [14], with components of the shuffle vectors normal to the twin plane. However, this would imply that the interface was a randomly curved continuum of high-index planes. Such a model could apply to massive transformations [80,81] for example, but it would be inconsistent with all known observations of twin interfaces with terraces separated by local defects. Instead, the shear-shuffle model is as follows. If the partials $\boldsymbol{b}_1$ glided directly, they would produce a high-energy stacking fault, which precludes such motion. They can move by one of two mechanisms. First, as described above, the partials could form by the emission of a pair of dislocations $\boldsymbol{b}_3 = \boldsymbol{k}_1$ and $\boldsymbol{b}_4 = \boldsymbol{k}_3$ (Figure 7(d)), which have equal and opposite screw components but same sign edge components that sum to $\boldsymbol{b}_1$. If one each is emitted into the twin and matrix, a misfit dislocation $\boldsymbol{b}_1$ is formed. If both ($\boldsymbol{b}_3 = \boldsymbol{k}_1$ and $\boldsymbol{b}_4 = \boldsymbol{k}_2$ or $\boldsymbol{b}_3 = \boldsymbol{k}_3$ and $\boldsymbol{b}_4 = \boldsymbol{k}_4$) emit into the same crystal, a disconnection with $\boldsymbol{b}_1$ is formed. The latter defect relaxes to the misfit dislocation by lateral sub-disconnection formation as discussed in [78,79]. The misfit dislocation can move by the reverse of this process. Obviously, there would be a barrier to this dissociation, and it may not be likely. A more plausible mechanism is that the defect moves by synchroshear [82–84]. Kronberg, Lann and Dubertret [83,84] propose synchroshear for $(\bar{1}012)$ twinning: here this is augmented by a specific TM mechanism. The correlation with step height is essentially a proof of the earlier proposal [83,84]. The component $\boldsymbol{k}$ vectors associated with synchroshear would be those shown in Figure 2(c). This defect could

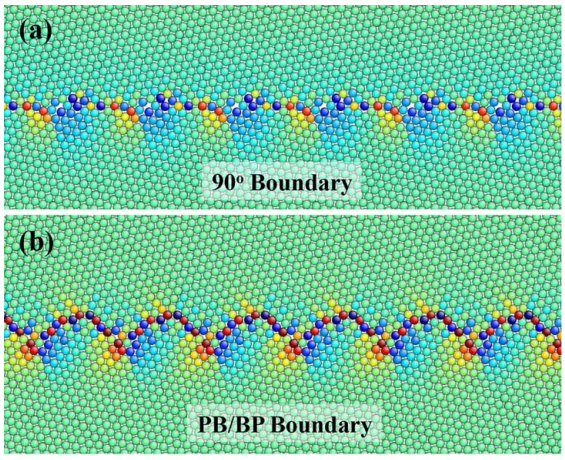

Figure 8. Atomic structures of the interfaces, (a) 90° tilt boundary (b) PB/BP faceted boundary. Atoms are colored according to their excess energy.

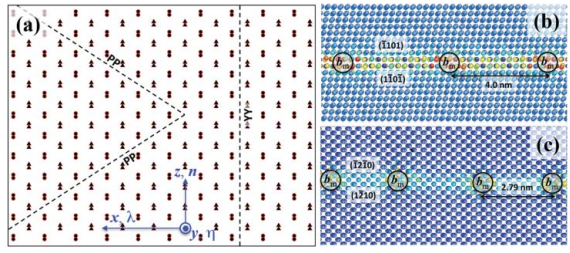

Figure 9. (a) The CDC of $\{\bar{1}012\}$ twins viewed along the forward $\boldsymbol{\eta}$ direction $[10\bar{1}1]$, corresponding to the DS view, showing two possible crystallographic interfaces: (b) the relaxed atomic structure of a twist pyramidal-pyramidal boundary (YY) and (c) relaxed atomic structure of a twist prismatic-prismatic boundary (PP). The symbol b_m represents misfit dislocation. Atoms are colored according to the excess energy. The interface region between misfit dislocations is coherent. $\boldsymbol{\xi}$ points toward the reader.

move by synchroshear as a single entity, with Burgers vector $\boldsymbol{b}_1$ equal to half the sum of two nonparallel $\boldsymbol{k}$ vectors. The defect moves without dissociation, and would leave no fault in its wake. With an increase in the thickness of a growth twin, the BP and PB disclination dipoles shown in Figure 5(b) could also be relaxed by the same mechanism of $\boldsymbol{b}_1$ emissary dislocations as illustrated in Figure 7(d).

We further investigated the atomic structures of the two most stable interfaces that are relaxed at zero temperature. Their total energies, elastic fields of dislocations plus coherent terrace energy, normalized to the mean horizontal areas, are 324 mJ/m^2 for the 90° tilt boundary (Figure 8(a)) and 223 mJ/m^2 for the PB/BP faceted boundary (Figure 8(b)). The local deviation from planarity arises because of core spreading and the short-range interaction between misfit dislocations and opposite sign TD dislocations. The 45° boundaries are favored because of their low energy.

3.3. Relaxed lateral TBs

For lateral interfaces, the TD sequences are the same as for the forward interfaces, but the character of the Burgers vectors changes to screw or mixed depending on the lateral boundary. For the hcp structure, crystallographic analysis suggests a cubic cross-section for a twin (Figure 1(d)). Figure 9(a) shows a dichromatic complex of $\{\bar{1}012\}$ twins viewed along the twinning shear direction $[10\bar{1}1]$, corresponding to the DS view. Lateral-TBs could have two possible interfaces: a twist pyramidal-pyramidal boundary (YY), $\{0\bar{1}11\}||\{01\bar{1}\bar{1}\}$ or $\{\bar{1}101\}||\{1\bar{1}0\bar{1}\}$ and $[10\bar{1}1]||[\bar{1}01\bar{1}]$ in the interface, and a twist prismatic-prismatic boundary (PP), $\{1\bar{2}10\}||\{\bar{1}2\bar{1}0\}$ and $[10\bar{1}1]||[\bar{1}01\bar{1}]$ in the interface, both favored because of the high commensurate degree of the two paired atomic planes. In either coherent case, the periphery of the lateral plane contains the twist Frank vector $\mathbf{f}_t$.

We studied the atomic structures of both YY and PP boundaries using empirical interatomic potential for Mg. The PP interface has an interfacial energy of 212 mJ/m^2, which is lower than most symmetrical tilt GBs [85], while YY has the higher interfacial energy of 318 mJ/m^2, which is greater than most tilt GBs [85]. Figure 9(b,c) shows the atomic structures of YY and PP interfaces, indicating the formation of semi-coherent interface and misfit dislocations. We focus on the PP interface because of its lower interface energy. Supporting this view, the pattern of Figure 10(a,b) indicate a misfit vector $\boldsymbol{b}_1$ for Mg. The Frank formula predicts the mean separation to be $d_1 = 2.82$ nm between these misfit dislocations, which is consistent with our MD result, $d = 2.79$ nm.

A reference CDP for the PP case is constructed in Figure 10(a), where the coherency strain is partitioned between the crystals, as indicated in the rotated CDP [17,86,87] defined in Figure 10(b). The PP interface has a relative rotation of unit cells of 90°. On the lateral surface the TD vectors $\boldsymbol{b}_t$ are left-handed screws with lines parallel to $\boldsymbol{\eta}$. These can then be smeared into a Bilby interface. Where the lateral surface terminates at the corner with the forward interface, normal to $\boldsymbol{\eta}$, they form a twist disclination of angle 3.71°, partitioned as a disclination dipole. These disclinations can be accommodated by collinear right-handed misfit screws with $\boldsymbol{b}_1 = 1/2[\bar{1}011]$ as shown in the $-\boldsymbol{\lambda}$, DS, view in Figure 10(c). This misfit array forms a pair of partitioned disclination dipoles with angle $-3.71°$ that cancels the stress field of the TD array (Figure 10(d)). Molecular statics simulations confirm this analysis. Figure 10(e) shows a DS view of a growth twin that comprises 60 atomic planes. The twin is surrounded by two CTBs and two PP boundaries. The emerging screws are revealed at the sides. As for the

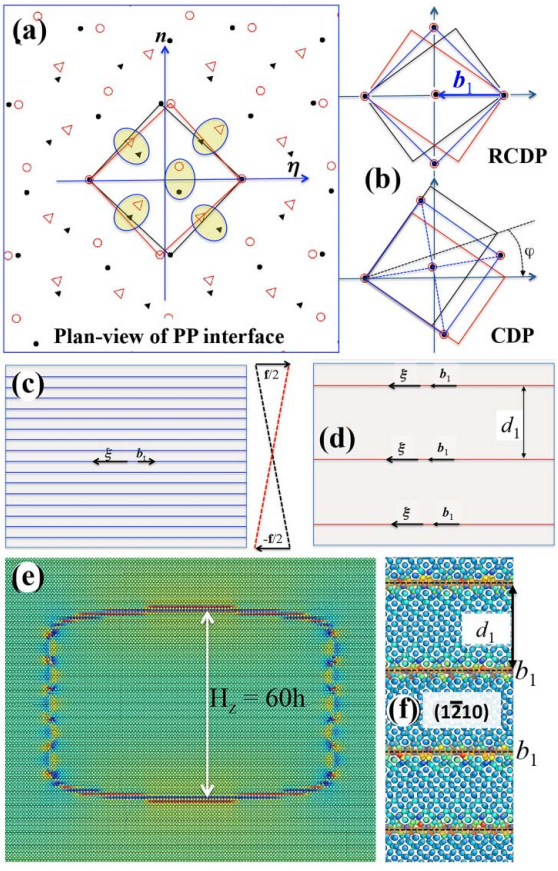

Figure 10. Crystallographic analysis of PP interface. (a) Lateral **λ** view of PP interface showing a CDC of two prismatic planes from the twin domain (red empty symbols) and the matrix (black solid symbols). Normal to z is a {01$\bar{1}$2} twin plane. The red rectangle and the black rectangle represent unit hexagonal cells. The shadowed region indicates that the two atoms will occupy the same position after atoms shuffle. (b) CDP indicates the CDP of a PP interface associated with a twist rotation of 90°. The disclination twist angle is $\varphi = 3.71°$. The disclination characteristics are revealed in the rotated coherent dichromatic pattern (RCDP). (c) The pileup of TDs on the lateral-TB, causing a twist angle 3.71° associated with a disclination dipole, and (d) relaxation of the disclination dipole by collinear right-handed misfit screws $\boldsymbol{b}_1$. (e) Atomic structure of a 60-atomic planes twin in the DS view, with misfit dislocations $\boldsymbol{b}_1$ on the $-\boldsymbol{\lambda}$ lateral DS view, visible only at the sides. Atoms are colored according to the local hydrostatic pressure. (f) Forward $-\boldsymbol{\lambda}$ view of PP interface showing emerging misfit screws at the sides. $\boldsymbol{\xi}$ points toward the reader.

edge arrays, misfit dislocations $\boldsymbol{b}_1$ are equal in magnitude to 15 TD vectors and produce a stress-free step when superposed.

4. Deformation twins

4.1. Twin shape

As already mentioned, the high driving force conditions under which deformation twins form are such that once a twin with a given TD forms, rapid multiplication of TDs with that specific $\boldsymbol{b}_t$ ensues, producing a stressed pileup type array. There is extensive evidence supporting such a view, including molecular dynamic simulations [19,21,31,39–41,48–50,58,66,88], shear offsets of defects serving as markers, e.g. Figures 43 and 45 in [8], the lenticular shape observed for such twins, e.g. Figure 42 in [8], and theoretical analysis [41,89,90]. As suggested and verified by atomistic simulations [91,92], TDs attract at short range and accumulate into discontinuous pileup configurations up to a nm or two in height. The constituent dislocations all have the same $\boldsymbol{b}_t$ and the pileup is therefore symmetric, as illustrated in Figure 11. Such a limited height step or the tip of a thin twin has been observed in atomistic simulations [50,51,88] and experiments [63,65]. Figure 12 is a plot of the variation of PB or BP step/facet heights in Mg and Co [60,62–65,93,94]. Significantly, many have heights other than the stress-free height: they have Burgers vector content. The coherent PB facets are no longer glissile in the *y*-direction. As verified in atomistic simulations [21,32,58,66], they can

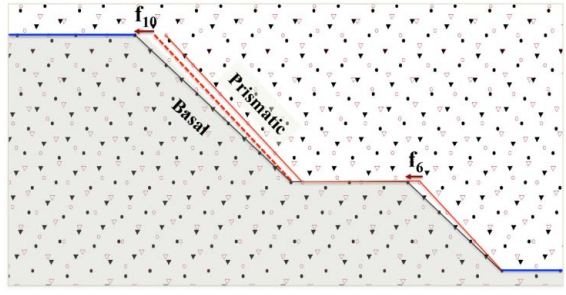

Figure 11. Schematic illustration of PB facets on a normal-TB viewed in the in the $-\boldsymbol{\lambda} = [\bar{1}\bar{1}20]$ direction. Facets with variable height form with disclination character represented by Frank vectors. $\boldsymbol{\xi}$ points toward the reader.

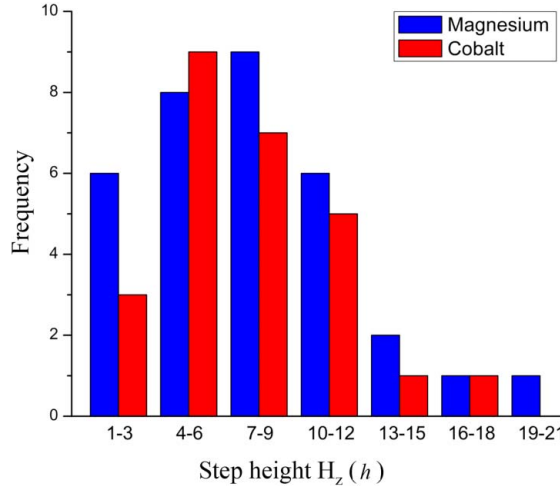

Figure 12. A distribution of PB and BP step heights in Mg and Co [60,62–65,93,94].

only move by the nucleation of TD pairs that sweep the facet and cause it to advance by one atomic unit in the y-direction.

4.2. Twin nucleation

Twin nuclei, whether formed homogeneously or heterogeneously, are bounded by CPB and CBP interfaces [32,60,94] with attendant large coherency stresses (Figure 6(d)) partitioned to the nucleus because of the stiffness of the matrix. In addition, there are local stresses associated with domain disclinations at the corners, characterized in Figure 6(a). The surface-to-volume ratio varies as $1/<r>$, where $<r>$ is the mean particle radius. For small $<r>$ the surface term dominates and the lower interfacial energy of the coherent interfaces causes the initial nucleus to be coherent as is common for all nucleation processes [15,95]. This remains true in the initial stages of growth, which occurs by the nucleation and propagation of TD pairs on the PB or BP interfaces. The details of the interactions at the corners are complex [8] and we give an overview here rather than the detail. With growth, analogous to the Frank analysis for crystal growth [96], the PB and BP facets grow faster (Figure 13(b–d)), implying easier nucleation/propagation of TD pairs on PB than on $(\bar{1}012)$. This leaves the coherent twin bounded by slower growing $(\bar{1}012)$ twin planes. The growing twin then forms the usual lenticular shape, Figure 13(e), with CTB terraces separated by TDs. This is consistent with the twin morphology found in bulk samples [69].

The relative magnitudes of the TD Burgers vectors for Mg on the twin plane, 0.049 nm and on the P/B facets, 0.148 nm [30], imply smaller formation energy for TDs on the twin plane. Contrariwise, the larger shuffle vectors and the greater number of shuffles for TDs on the twin plane would favor a lower Peierls stress for TDs on the facet. The observations favor the latter as the governing process for twin propagation, a model suggested in [21].

For slower growing twins, with less driving force, once the bulk elastic energy term becomes dominant with increasing $<r>$, the time scale is such that it becomes favorable to nucleate misfit defects to reduce the elastic fields. The twin still grows by TD pair nucleation. The misfit dislocations are glissile normal to the interface and so can advance by one unit in the z-direction as a TD passes them. However, there is a local elastic interaction between the TD and the misfit dislocation; so there is some pinning interaction. This motion of a relaxed interface process is more characteristic of growth or annealing twins during the twinning process. The same structures can form, however in the recovery stage for the deformation twins.

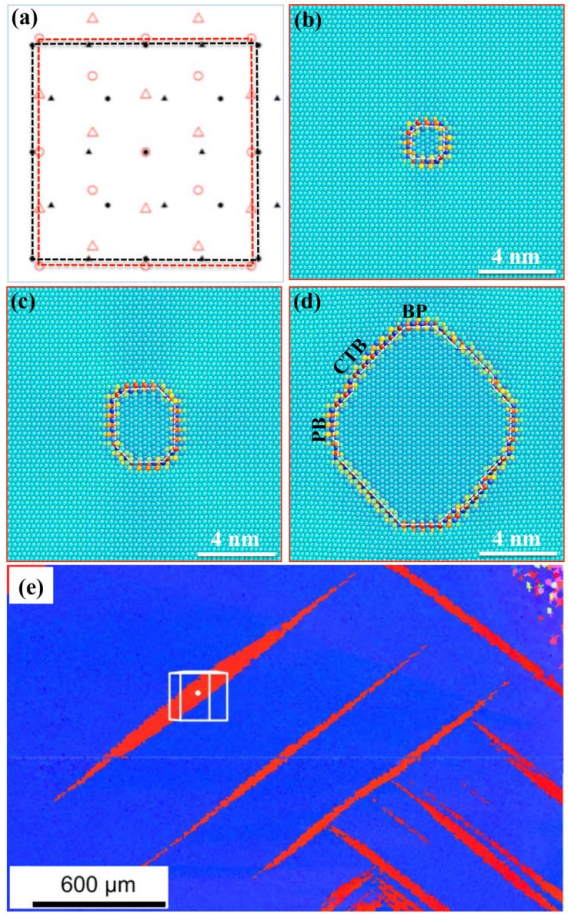

Figure 13. (a) Double CDPs for a $(10\bar{1}2)$ twin that is surrounded by PB and BP interfaces. (b) Relaxed atomic structure of a twin nucleus, showing twin growth from PB dominated to CTB dominated boundary. Atoms are colored according their excess potential energy. (e) EBSD image showing lenticular shape of $(10\bar{1}2)$ twins in Mg.

The view of the lateral-TB is similar but the TDs Burgers vectors have screw character, corresponding to a cubic cross-section of the twin nucleus (Figure 1(d)). In the coherent state the twin can grow in the lateral direction as well by propagation of the TD pairs exactly analogous to the growth in the forward and normal directions described above.

5. Recovered deformation twins

Given time the lenticular twins with stressed TD arrays as discussed above recover by the addition of misfit defects that cancel the coherency stress fields. This can occur by the nucleation of emissary dislocations to create relaxed structures similar to those in Figure 7. Even with a small driving force, TDs can accumulate and form PB or BP facets. As more TDs accumulate, the Frank vector associated with the facet increases as a function of the step

height. When the step height becomes greater than 15 atomic planes in Mg, the Frank vector becomes greater than the edge component of a $\boldsymbol{b}_1$ dislocation and a misfit dislocation with this vector can form, as shown in Figure 7(d). As discussed for step motion, the emitted dislocations can be a set of $\boldsymbol{a}$-type dislocations or can be a synchroshear defect with a net Burgers vector $\boldsymbol{b}_1$. Thus, if the twin or step height is a multiple of 15 planes, a pure step or a step-free twin front can form. For all other step heights, the TD (or twin front) has both dislocation and step character.

The relaxation of coherency stress and the resulted pinning on the lateral boundary are also attributed to misfit dislocations in the lateral-TB. The coherency stress fields associated with the pileup of screw TDs on the lateral boundary can be relaxed in two ways. The TD left-handed screw dislocations $\boldsymbol{b}_t$ deposit on the lateral surface, Figure 14(a), forming an array equivalent to a twist disclination with an angle $\varphi = 3.71°$. Then, Figure 14(b), misfit dislocations $\boldsymbol{b}_1 = 1/2[\bar{1}011]$ are emitted by synchroshear, swing around in the twin or matrix and deposit on the lateral PP face as right-handed screw misfit dislocations, equivalent to a twist disclination with an angle $-3.71°$, which exactly cancels the field of the left-handed twist disclination. The alternative entails emission of a-type dislocations, Figure 14(c). These a-type dislocations also swing around, and deposit on the PP surface as misfit mixed dislocations with right-handed screw components, Figure 14(c). The edge components are equal and opposite so the total edge component of **B** is zero. At long range, the field of the cross grid of screws is

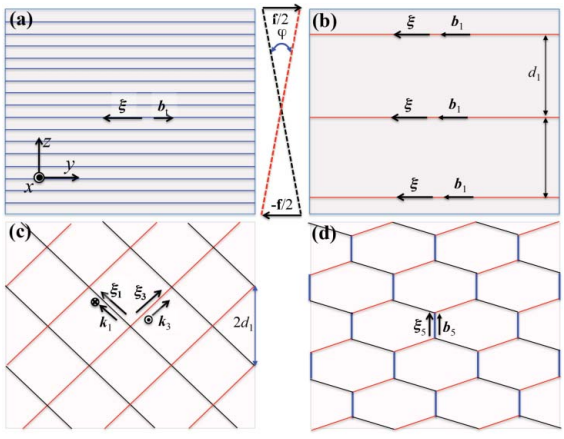

Figure 14. Relaxation mechanisms of lateral-TB. (a) TD dislocations $\boldsymbol{b}_t$ deposited on lateral surface. (b) Misfit dislocations $\boldsymbol{b}_1$ formed by synchroshear and deposited on lateral boundary. (c) Emissary dislocations $\boldsymbol{b}_3 = \boldsymbol{k}_1$ and $\boldsymbol{b}_4 = \boldsymbol{k}_3$ that have deposited on the lateral boundary. (d) Reaction of Figure (c) at nodes, eventually leading to a vertical array of misfit dislocations $\boldsymbol{b}_5 = \boldsymbol{k}_1 + \boldsymbol{k}_3 (= \boldsymbol{b}_1 = 1/2[10\bar{1}1])$.

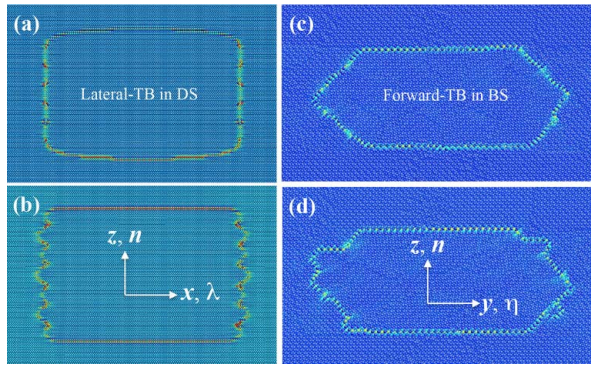

Figure 15. Atomistic simulations of the propagation of relaxed TBs. (a) Initial structure of relaxed lateral-TB, and (b) formation of steps due to the pinning of interface dislocations. (c) Initial structure of relaxed forward-TB, and (b) formation of steps due to the pinning of interface dislocation. Atoms are colored according to their excess energy.

equivalent to two arrays of right-handed screws parallel to the z-axis. Together, these right-handed screw arrays have a misfit disclination field that cancels that of the $\boldsymbol{b}_t$ array (orthogonal screws of equal strength and opposite character produce a pure twist disclination [97]). These could further interact to reduce total line length and form the arrays in Figure 14(d), with two sets of right-handed screws $\boldsymbol{b}_1$. Either of these latter arrays also fully relieves the disclination stresses [14]. Based on observations and simulations, the first mechanism exists, but the second is predominant.

For any of these mechanisms, there is some pinning on the forward interface at points where the TDs and misfits intersect because of the core-type interactions. There is also pinning on the lateral interface, since there is a longer-range attraction between opposite sign screws as well as a local core-type interaction. Consequently, the situation is as shown in Figure 15. For either the 90° tilt or the 45° inclined arrangements, Figure 15(a,c), the twins are fully relaxed after recovery. With a stress then applied growth occurs by TD pair formation, but there is pinning at intersections and the interface becomes ragged, Figure 15(b,d).

6. Discussion

6.1. Types of interface

We see that there are many different interface types and configurations. For rapidly formed deformation twins, only one type of TD is present and the interface has associated large stresses, causing the twin to have a lenticular shape with the TDs in a pile-up configuration. At the atomic scale there is a short-range attraction between TDs, and this favors accumulation of the TDs into mainly

slanted PB or BP facets, but square facets are also possible. These facets have disclination character, with associated strain fields. If a stress is applied to such an array, the facets can continue to move via TD pair nucleation and lateral TD propagation (analogous to the kink pair mechanism for dislocation motion). The terraces between facets can also move by TD pair motion. This is completely consistent with both the classical view [6,11] and the recent TM model [8]. The TDs have either dislocation or disclination character, depending on step height, and move, leaving coherent terraces in their wake.

Growth or annealing twins also have steps or forward interfaces that can be quite large in magnitude, have 90° or 45° orientations, and have misfit arrays that fully relax stresses.

Recovered deformation twins have configurations and sizes similar to the deformation structures but with all unit TDs gathered into facets. These can be fully relaxed (pure steps) only for specific step heights, multiples of $H_z = 15h$ for both square steps and PB/BP facets in the case of Mg. Under stress the incompletely relaxed disconnections experience a Peach–Koehler force and can move under that driving force. The pure steps can also move under the weaker driving force of a strain-energy density gradient. Li and coworkers [49,98] promulgate a pure shuffle mechanism that differs.

6.2. The shear-shuffle mechanism

The above analysis shows that, like many other macroscopic observations, HRTEM and atomistic simulations agree with the shear-shuffle classical [6,11,35] and TM models [8,17,27,37]. For large pure steps, motion entails pure glide-shuffle, which is essentially a limiting form of TD motion. This glide-shuffle model differs from the general shuffle promulgated by Li and coworkers [49,98].

The last of the pure shuffle treatments [49] summarizes the earlier work and we address the model and conclusions presented there. The basis for the proposal is the observation of a PB facet with no other defects present [49]. The TEM micrographs and analysis in [60,62–65,93–95] show PB facets with varying sizes, Figure 12, many of which are not pure steps, i.e. not 15 or 30 planes high. However, the maximum in the step distribution in Figure 12 is for the pure step height of 15 planes; so pure steps formed by glide-shuffle are present. All other cases represent TDs with both dislocation and step character, and these often form together with pure steps on the same interface. The observation of a pure step may or may not indicate that it formed during deformation. Indeed, it is more likely that the pure steps form by recovery, entailing emissary dislocations. Pure steps can move by a glide-shuffle mechanism, consistent with the TM, but not consistent with a general shuffle mechanism.

General shuffle could occur when there are no terraces, as for massive transformations, but there are no known twins that move by such a mechanism. For a shuffle mechanism other than that for pure steps, the interface cannot contain coherent terraces (or there would be dislocation content). Incoherent terraces would have high-index character and would be unstable as described next. The interface would have to be randomly curved and high index as for massive transformations and for grain growth. The Gibbs–Wulff equilibrium shape for such a twin would be equiaxed, a sphere in the interfacial energy plot as a function of orientation. Thus, it is essentially impossible that a lenticular shape twin could form by pure shuffle. The nucleus for a twin has been seen to form by general shuffle [32]. This occurs because the coherent nucleus energy is dominated by the surface energy. As the nucleus grows, the bulk energy becomes dominant and defects (TDs for twins, other defects in general) that minimize increases in coherency strain become dominant [8,99,100].

Recovered interfaces can have misfit dislocations with out-of-plane Burgers vectors producing tilt. Thus, it is consistent with the TM that measurements indicate a spread of orientation relations about the ideal value. The ideal value always applies for terraces.

6.3. Twinning in nano-sized single crystals

Recently, in situ TEM studies of twinning in nano-sized single crystals found that twin propagates mainly through migration of PB/BP boundaries [60], suggesting that deformation twinning seems related to sample dimensions. The deformed TEM sample does not show obvious geometric shear along the twinning shear. The primary TB comprises PB and BP steps and deviates from the twin plane. Atomistic simulations confirmed the motion of PB/BP interfaces under a stress normal to the interface [32,58]. Based on these observations, Prism↔Basal transformation mechanism was proposed for twin growth [58,60,93]. The resultant extension strain 6.5% in one direction (Basal → Prism) and contraction strain −6.5% in the orthogonal direction (Prism → Basal) together are equivalent to a shear strain associated with the twinning shear. According to the crystallography of the twin, the normal stress σ_{PB} on the PB interface generates the resolved shear stress τ_{CTB} (approximately equals to $0.5\sigma_{PB}$) on the twin plane. It is noticed that the normal stress is close to 230–280 MPa in their experiments, corresponding to the resolved shear stress $\tau_{CTB} = 115 - 140$MPa, which is much higher than the critical twinning shear stress (20–40 MPa) in the bulk

sample. In addition, the strain-hardening rate, 3–4 GPa measured in their experiments associated with the migration of PB/BP interfaces, is significantly higher than the strain-hardening rate (a few MPa) associated with twinning in the bulk sample [100].

These quantitative differences observed in nano-sized single crystals from bulk sample can be accounted for by nucleation and growth mechanisms discussed in Section 4. Twin nuclei are bounded by CPB and CBP interfaces [32,60,94] with attendant large coherency stresses (Figure 6(d)) partitioned to the nucleus in a bulk sample because of the stiffness of the matrix. However for nano-sized single crystals, the large coherency stresses associated with CPB and CBP boundaries will be partitioned to the matrix due to free surfaces and relaxed by misfit dislocations on PB/BP boundaries. These misfit dislocations are formed associated with the nucleation and emission of lattice dislocation with Burges vector $<a>$ on PB/BP interfaces. The nucleated dislocation glides on the basal plane into the matrix and the residual is left on the PB/BP interfaces (acting as misfit dislocation). When the twin is in a bulk sample that is subjected to effective tensile stress along the $<c>$ axis, the resolved shear stress on the basal plane is equal to zero. The emission of $<a>$ dislocations from PB/BP interface into the matrix is unfavorable, which precludes formation of long PB/BP interfaces. However, when the sample is nano-sized single crystal with free surfaces, the image force due to free surfaces drives $<a>$ dislocations out of the sample, facilitating the formation of long PB/BP interfaces. Correspondingly, TB comprises long PB/BP interfaces with misfit dislocations. Twin growth is accomplished through the nucleation and propagation of TD pairs on the PB or BP interfaces. Misfit dislocations pin the migration of PB/BP interfaces, accounting for the high strain-hardening rate.

7. Conclusions

Taking $\{\bar{1}012\}\langle 10\bar{1}1\rangle$ twins in Mg as a representative model system, we systematically investigated equilibrium and non-equilibrium boundaries associated with $\{\bar{1}012\}$ growth/annealing and deformation twins. Corresponding to the three-dimensional 'normal', 'forward' and 'lateral' propagation of a twin, three TBs are crystallographically designated as normal-TB, forward-TB and lateral-TB. Intrinsic defects and interface structure associated with the three TBs are characterized at the atomic level through HRTEM and atomistic simulations, interpreted by the TM.

Growth and annealing twins have zero or very small elastic stresses/strains. TBs can be considered as equilibrium or near-equilibrium boundary with respect to elastic strain energy. For a stress-free condition, a twin has a specific thickness, and a step on a TB has a specific height. The specific thickness varies with material. The minimum thickness is 15 atomic planes for Mg. The normal TBs usually have perfect twin planes or large perfect terraces. The forward TBs have either 45° BP or PB facets or 90° walls, each comprising of TDs and misfit dislocations that have zero net Burgers vector. The lateral-TB is a twist prismatic-prismatic boundary (PP), $\{1\bar{2}10\}||\{\bar{1}2\bar{1}0\}$. Emissary dislocations deposit on the lateral interface. They have zero stress screw arrays consisting of left-handed TDs and right-handed misfit dislocations.

Deformation twins often contain only one type of TD and have associated elastic strain fields. Corresponding to the unidirectional shear, a characteristic shear strain is directly associated with twinning. In an elastic equilibrium point of view, the internal stress inside twins is different than in the surrounding medium. The resulting internal stress in the surrounding medium intrinsically prevents the twin from growing [101,102]. But it does not change twinning mechanisms. Associated with P/B facets, a new type of disclination, a glide disconnection, is defined. The forward-TB contains edge TDs and the lateral-TB contains screw TDs, and they have associated stress fields. When there is adequate time, the twins with stressed TD arrays recover by the addition of misfit defects that cancel the coherency stress fields. The resultant structures resemble those of the growth/annealing twins. The formation of misfit defects is associated with the nucleation and emission of dislocations from interface into the twin and the surrounding medium. The associated difference in internal stress between the interior of the twin and the surrounding matrix will affect the recovery of stressed TDs arrays, as discussed in Section 4.2.2. The most consistent interpretation of recovered steps for the $\{\bar{1}012\}\langle 10\bar{1}1\rangle$ twins is that the formation of misfit defects entails synchroshear, as would the motion of the defects when the interface moves.

Our results for twinning and twin structures are consistent with classical models and the TM in that the mechanism is one of shear-shuffle associated with the motion of TDs. The exception is for large pure steps that can move solely by glide-shuffle, also consistent with the TM, but not consistent with a general shuffle mechanism.

Disclosure statement

No potential conflict of interest was reported by the authors.

Funding

This work is supported by the US National Science Foundation (NSF-CMMI) under grant No. 1661686. Gong and

Wang acknowledge the support by the Nebraska Center for Energy Sciences Research (26-1217-0020-213), University of Nebraska-Lincoln. Gong, Hirth, Wang and Liu acknowledge the support by the the Office of Basic Energy Sciences, Project FWP 06SCPE401, under US DOE contract no. W-7405-ENG-36. Shen acknowledges the support by the National Science Foundation of China Grant No. 51471107 and 51671132, CCS project Grant No. YK 2015-0202002. JW and JPH thank Prof. Robert Pond for his valuable comments and suggestions.

ORCID

Jian Wang http://orcid.org/0000-0001-5130-300X

References

[1] Bufford D, Liu Y, Wang J, et al. In situ nanoindentation study on plasticity and work hardening in aluminium with incoherent twin boundaries. Nat Commun. 2014;5:1–9.
[2] Wang J, Anderoglu O, Hirth JP, et al. Dislocation structures of Σ3 {112} twin boundaries in face centered cubic metals. Appl Phys Lett. 2009;95:021908.
[3] Zhang X, Misra A, Wang H, et al. Nanoscale-twinning-induced strengthening in austenitic stainless steel thin films. Appl Phys Lett. 2004;84:1096–1098.
[4] Li X, Wei Y, Lu L, et al. Dislocation nucleation governed softening and maximum strength in nano-twinned metals. Nature. 2010;464:877–880.
[5] Wang YM, Sansoz F, LaGrange T, et al. Defective twin boundaries in nanotwinned metals. Nat Mater. 2013;12:697–702.
[6] Booth M, Randle V, Owen G. Time evolution of Σ3 annealing twins in secondary recrystallized nickel. J Microsc. 2005;217:162–166.
[7] Fullman RL, Fisher JC. Formation of annealing twins during grain growth. J Appl Phys. 1951;22:1350–1355.
[8] Hirth JP, Wang J, Tomé CN. Disconnections and other defects associated with twin interfaces. Prog Mater Sci. 2016;83:417–471.
[9] Wang J, Li N, Misra A. Structure and stability of Σ3 grain boundaries in face centered cubic metals. Philos Mag. 2013;93:315–327.
[10] Li N, Wang J, Misra A, et al. Twinning dislocation multiplication at a coherent twin boundary. Acta Mater. 2011;59:5989–5996.
[11] Cottrell AH, Bilby BA. LX. A mechanism for the growth of deformation twins in crystals. Lond Edinb Dubl Phil Mag. 1951;42:573–581.
[12] Sleeswyk AW. Perfect dislocation pole models for twinning in the fcc and bcc lattices. Philos Mag. 1974;29:407–421.
[13] Venables JA. On dislocation pole models for twinning. Philos Mag. 1974;30:1165–1169.
[14] Hirth JP, Lothe J. Theory of dislocations. 2nd ed. New York: Wiley; 1982.
[15] Russell KC, Aaronson HI. Sequences of precipitate nucleation. J Mater Sci. 1975;10:1991–1999.
[16] Thompson N, Millard DJ. XXXVIII. Twin formation, in cadmium. Lond Edinb Dubl Phil Mag. 1952;43:422–440.
[17] Hirth JP, Pond RC, Hoagland RG, et al. Interface defects, reference spaces and the Frank-Bilby equation. Prog Mater Sci. 2013;58:749–823.
[18] Hirth JP, Pond RC. Steps, dislocations and disconnections as interface defects relating to structure and phase transformations. Acta Mater. 1996;44:4749–4763.
[19] Barrett CD, El Kadiri H. The roles of grain boundary dislocations and disclinations in the nucleation of {10$\bar{1}$2} twinning. Acta Mater. 2014;63:1–15.
[20] Serra A, Bacon DJ. A new model for {10$\bar{1}$2} twin growth in hcp metals. Philos Mag A. 1996;73:333–343.
[21] Serra A, Pond RC, Bacon DJ. Computer simulation of the structure and mobility of twinning dislocations in H.C.P. metals. Acta Metall Mater. 1991;39:1469–1480.
[22] Tu J, Zhang X, Wang J, et al. Structural characterization of {10$\bar{1}$2} twin boundaries in cobalt. Appl Phys Lett. 2013;103:051903.
[23] Wang J, Beyerlein IJ, Tomé CN. Reactions of lattice dislocations with grain boundaries in Mg: implications on the micro scale from atomic-scale calculations. Int J Plast. 2014;56:156–172.
[24] Wang J, Beyerlein IJ, Hirth JP, et al. Twinning dislocations on {$\bar{1}$011} and {$\bar{1}$013} planes in hexagonal close-packed crystals. Acta Mater. 2011;59:3990–4001.
[25] Hirth JP. Dislocations, steps and disconnections at interfaces. J Phys Chem Solids. 1994;55:985–989.
[26] Pond RC. Line defects in interfaces. In: Nabarro FRN, editor. Dislocations in solids. Vol. 8. Amsterdam: North-Holland; 1989. p. 1–66.
[27] Pond RC, Ma X, Chai YW, et al. Topological modelling of martensitic transformations. In: Nabarro FRN, Hirth JP, editors. Dislocations in solids. Vol. 13. Amsterdam: North-Holland; 2007. p. 225–262.
[28] Fullman RL. Interfacial free energy of coherent twin boundaries in copper. J Appl Phys. 1951;22:448–455.
[29] Yu Q, Wang J, Jiang Y, et al. Twin-twin interactions in magnesium. Acta Mater. 2014;77:28–42.
[30] Ostapovets A, Serra A. Characterization of the matrix–twin interface of a (10$\bar{1}$2) twin during growth. Philos Mag. 2014;94:2827–2839.
[31] Xu B, Capolungo L, Rodney D. On the importance of prismatic/basal interfaces in the growth of twins in hexagonal close packed crystals. Scr Mater. 2013;68:901–904.
[32] Wang J, Yadav SK, Hirth JP, et al. Pure-shuffle nucleation of deformation twins in hexagonal-close-packed metals. Mater Res Lett. 2013;1:126–132.
[33] Liu Y, Li N, Shao S, et al. Characterizing the boundary lateral to the shear direction of deformation twins in magnesium. Nat Commun. 2016;7:1–6.
[34] Bilby BA, Crocker AG. The theory of the crystallography of deformation twinning. Proc R Soc A. 1965;288:240–255.
[35] Kelly AA, Knowles KM. Crystallography and crystal defects. 2nd ed. New York: Wiley; 2012.
[36] Christian JW, Mahajan S. Deformation twinning. Prog Mater Sci. 1995;39:1–157.
[37] Howe JM, Pond RC, Hirth JP. The role of disconnections in phase transformations. Prog Mater Sci. 2009;54:792–838.

[38] Serra A, Bacon DJ, Pond RC. The crystallography and core structure of twinning dislocations in h.c.p. metals. Acta Metall. 1988;36:3183–3203.
[39] Barrett CD, El Kadiri H. Impact of deformation faceting on {10$\bar{1}$2}, {10$\bar{1}$1} and {10$\bar{1}$3} embryonic twin nucleation in hexagonal close-packed metals. Acta Mater. 2014;70:137–161.
[40] Khater HA, Serra A, Pond RC. Atomic shearing and shuffling accompanying the motion of twinning disconnections in Zirconium. Philos Mag. 2013;93:1279–1298.
[41] Pond RC, Hirth JP, Serra A, et al. Atomic displacements accompanying deformation twinning: shears and shuffles. Mater Res Lett. 2016;4:185–190.
[42] Braisaz T, Ruterana P, Nouet G, et al. Investigation of {10$\bar{1}$2} twins in Zn using high-resolution electron microscopy: interfacial defects and interactions. Philos Mag A. 1997;75:1075–1095.
[43] Ezaz T, Sehitoglu H. Coupled shear and shuffle modes during twin growth in B2-NiTi. Appl Phys Lett. 2011;98:241906.
[44] Morrow BM, McCabe RJ, Cerreta EK, et al. Observations of the atomic structure of tensile and compressive twin boundaries and twin–twin interactions in zirconium. Metall Mater Trans A. 2014;45:5891–5897.
[45] Bao L, Schuman C, Lecomte JS, et al. A study of twin variant selection and twin growth in titanium. Adv Eng Mater. 2011;13:928–932.
[46] Barnett MR. Twinning and the ductility of magnesium alloys: (Part I): "tension twins". Mater Sci Eng A. 2007;464:1–7.
[47] Chichili DR, Ramesh KT, Hemker KJ. The high-strain-rate response of alpha-titanium: experiments, deformation mechanisms and modeling. Acta Mater. 1998;46:1025–1043.
[48] El Kadiri H, Barrett CD, Wang J, et al. Why are {10$\bar{1}$2} twins profuse in magnesium? Acta Mater. 2015;85:354–361.
[49] Li B, Zhang XY. Twinning with zero twinning shear. Scr Mater. 2016;125:73–79.
[50] Wang J, Hirth JP, Tomé CN. ($\bar{1}$012) Twinning nucleation mechanisms in hexagonal-close-packed crystals. Acta Mater. 2009;57:5521–5530.
[51] Wang J, Hoagland RG, Hirth JP, et al. Nucleation of a ($\bar{1}$012) twin in hexagonal close-packed crystals. Scr Mater. 2009;61:903–906.
[52] Serra A, Bacon DJ. Interaction of a moving {10$\bar{1}$2} twin boundary with perfect dislocations and loops in a hcp metal. Philos Mag. 2010;90:845–861.
[53] Hirth JP, Pond RC. Compatibility and accommodation in displacive phase transformations. Prog Mater Sci. 2011;56:586–636.
[54] Pond RC, Hirth JP. Defects at surfaces and interfaces. Solid State Phys. 1994;47:287–365.
[55] Chu HJ, Wang J, Beyerlein IJ. Anomalous reactions of a supersonic coplanar dislocation dipole: bypass or twinning? Scr Mater. 2012;67:69–72.
[56] Wang J, Misra A, Hirth JP. Shear response of Σ3{112} twin boundaries in face-centered-cubic metals. Phys Rev B. 2011;83:064106.
[57] Yu Q, Wang J, Jiang Y, et al. Co-zone {$\bar{1}$012} twin interaction in magnesium single crystal. Mater Res Lett. 2014;2:82–88.
[58] Wang J, Liu L, Tomé CN, et al. Twinning and de-twinning via glide and climb of twinning dislocations along serrated coherent twin boundaries in Hexagonal-Close-Packed metals. Mater Res Lett. 2013;1:81–88.
[59] Ostapovets A, Burščík J, Gröger R. Deformation due to migration of faceted {10$\bar{1}$2} twin boundaries in magnesium and cobalt. Philos Mag. 2015;95:4106–4117.
[60] Liu BY, Wang J, Li B, et al. Twinning-like lattice reorientation without a crystallographic twinning plane. Nat Commun. 2014;5:1–6.
[61] Kim I, Kim J, Shin DH, et al. Deformation twins in pure titanium processed by equal channel angular pressing. Scr Mater. 2003;48:813–817.
[62] Tu J, Zhang X, Ren Y, et al. Structural characterization of {10$\bar{1}$2} irregular-shaped twinning boundary in hexagonal close-packed metals. Mater Charact. 2015;106:240–244.
[63] Tu J, Zhang X, Zhou ZM, et al. Structural characterization of {10$\bar{1}$2} twin tip in deformed magnesium alloy. Mater Charact. 2015;110:39–43.
[64] Wang J, Beyerlein IJ, Hirth JP. Nucleation of elementary {$\bar{1}$011} and {$\bar{1}$013} twinning dislocations at a twin boundary in hexagonal close-packed crystals. Modell Simul Mater Sci Eng. 2012;20:024001.
[65] Sun Q, Zhang XY, Ren Y, et al. Interfacial structure of {10$\bar{1}$2} twin tip in deformed magnesium alloy. Scr Mater. 2014;90-91:41–44.
[66] Pond RC, Serra A, Bacon DJ. Dislocations in interfaces in the hcp metals—II. Mechanisms of defect mobility under stress. Acta Mater. 1999;47:1441–1453.
[67] Li YJ, Chen YJ, Walmsley JC, et al. Faceted interfacial structure of {10$\bar{1}$1} twins in Ti formed during equal channel angular pressing. Scr Mater. 2010;62:443–446.
[68] Wang J, Li N, Anderoglu O, et al. Detwinning mechanisms for growth twins in face-centered cubic metals. Acta Mater. 2010;58:2262–2270.
[69] Anderoglu O, Misra A, Wang H, et al. Epitaxial nanotwinned Cu films with high strength and high conductivity. Appl Phys Lett. 2008;93:083108.
[70] Dash S, Brown N. An investigation of the origin and growth of annealing twins. Acta Metall. 1963;11:1067–1075.
[71] Liu L, Wang J, Gong SK, et al. High resolution transmission electron microscope observation of zero-strain deformation twinning mechanisms in Ag. Phys Rev Lett. 2011;106:175504.
[72] Zhu YT, Liao XZ, Wu XL. Deformation twinning in nanocrystalline materials. Prog Mater Sci. 2012;57:1–62.
[73] Romanov AE, Vladimirov VI. Vol. 9: Dislocations and Disclinations. In Nabarro FRN, editor. Dislocations in Solids. Amsterdam, North-Holland: Elsevier Science. 1992. p. 192–302.
[74] Frank FC. I. Liquid crystals: on the theory of liquid crystals. Discuss Faraday Soc. 1958;25:19–28.
[75] Anthony K, Essmann U, Seeger A, et al. Disclinations and the Cosserat-continuum with incompatible rotations. In: Kröner E, editor. Mechanics of generalized continua. IUTAM Symposia (International Union of

Theoretical and Applied Mechanics). Springer, Berlin, Heidelberg; 1968. p. 355–358.
[76] Simmons JA, De Wit R., Bullough R, editors. Fundamental aspects of dislocation theory: conference proceedings. National Bureau of Standards, April 21-25, 1969. Washington (DC): US National Bureau of Standards, U.S. Government Printing Office; 1970.
[77] Hirth JP. A brief history of dislocation theory. Metall Trans A. 1985;16:2085–2090.
[78] Hirth JP, Pond RC, Lothe J. Disconnections in tilt walls. Acta Mater. 2006;54:4237–4245.
[79] Khater HA, Serra A, Pond RC, et al. The disconnection mechanism of coupled migration and shear at grain boundaries. Acta Mater. 2012;60:2007–2020.
[80] Aaronson HI. Mechanisms of the massive transformation. Metall Mater Trans A. 2002;33:2285–2297.
[81] Massalski TB. Massive transformations. Mater Sci Eng. 1976;25:119–125.
[82] Kronberg ML. Plastic deformation of single crystals of sapphire: basal slip and twinning. Acta Metall. 1957;5:507–524.
[83] Kronberg ML. A structural mechanism for the twinning process on $\{10\bar{1}2\}$ in hexagonal close packed metals. Acta Metall. 1968;16:29–34.
[84] Lann AL, Dubertret A. A development of Kronberg's model for $\{10\bar{1}2\}$ twins in HCP metals. Extension to $\{11\bar{2}2\}$ twins. Phys Status Solidi A. 1979;51:497–507.
[85] Wang J, Beyerlein IJ. Atomic structures of symmetric tilt grain boundaries in hexagonal close packed (hcp) crystals. Modell Simul Mater Sci Eng. 2012;20:024002.
[86] Wang J, Zhang R, Zhou C, et al. Characterizing interface dislocations by atomically informed Frank–Bilby theory. J Mater Res. 2013;28:1646–1657.
[87] Wang J, Zhang RF, Zhou CZ, et al. Interface dislocation patterns and dislocation nucleation in face-centered-cubic and body-centered-cubic bicrystal interfaces. Int J Plast. 2014;53:40–55.
[88] Kucherov L, Tadmor EB. Twin nucleation mechanisms at a crack tip in an hcp material: molecular simulation. Acta Mater. 2007;55:2065–2074.
[89] Ostapovets A, Molnár P. On the relationship between the "shuffling-dominated" and "shear-dominated" mechanisms for twinning in magnesium. Scr Mater. 2013;69:287–290.
[90] Serra A, Bacon DJ, Pond RC. Comment on "atomic shuffling dominated mechanism for deformation twinning in magnesium". Phys Rev Lett. 2010;104:029603.
[91] Enomoto M, Hirth JP. Computer simulation of ledge migration under elastic interaction. Metall Mater Trans A. 1996;27:1491–1500.
[92] Kamat SV, Hirth JP, Müllner P. The effect of stress on the shape of a blocked deformation twin. Philos Mag A. 1996;73:669–680.
[93] Liu BY, Wan L, Wang J, et al. Terrace-like morphology of the boundary created through basal-prismatic transformation in magnesium. Scr Mater. 2015;100:86–89.
[94] Zhang X, Misra A. Superior thermal stability of coherent twin boundaries in nanotwinned metals. Scr Mater. 2012;66:860–865.
[95] Olson GB, Cohen M. A general mechanism of martensitic nucleation: part I. General concepts and the FCC → HCP transformation. Metall Trans A. 1976;7:1897–1904.
[96] Frank FC, Ives MB. Orientation-dependent dissolution of germanium. J Appl Phys. 1960;31:1996–1999.
[97] Hirth JP. Stabilization of strained multilayers by thin interlayers. J Mater Res. 1993;8:1572–1577.
[98] Li B, Ma E. Atomic shuffling dominated mechanism for deformation twinning in magnesium. Phys Rev Lett. 2009;103:035503.
[99] Wang J, Yu Q, Jiang Y, et al. Twinning-associated boundaries in hexagonal close-packed metals. JOM. 2014;66(1):95–101.
[100] Liao X, Wang J, Nie J, et al. Deformation twinning in hexagonal materials. MRS Bull. 2016;41(4):314–319.
[101] Kumar MA, Beyerlein IJ, McCabe RJ, et al. Grain neighbour effects on twin transmission in hexagonal close-packed materials. Nat Commun. 2016;7:13826.
[102] Xu S, Gong M, Schuman C, et al. Sequential $\{10\bar{1}2\}$ twinning stimulated by other twins in titanium. Acta Mater. 2017;132:57–68.